

M.J. SZCZERBA^{1*}, M. KOWALSKA¹, M. DUDZIŃSKI¹,
A. WIERZBICKA-MIERNIK¹, Ł. ROGAL¹, A. BIGOS¹

EFFECT OF ANNEALING ON MICROSTRUCTURE AND FUNCTIONAL PROPERTIES OF Ni-Mn-Ga-Cu ALLOYS PRODUCED BY MELT SPINNING TECHNIQUE

In this work, we have performed experimental measurements and analysis of the annealing effect in the temperature range of 100°C-900°C on the magnetic field-induced bending phenomenon of Heusler alloys with the nominal composition of Ni₅₀Mn₃₀Ga₁₈Cu₂. The annealing process resulted in an increase of the average grain size. Annealing also affected the magnetic field-induced bending effect, increasing the maximum value of the obtained normalized deflection by about six-fold. However, this effect occurred in the case of ribbons annealed at higher temperatures, i.e. above 500°C. Annealing also led to a reduction in the magnetic field value required to activate the magnetic field-induced bending effect. The annealing process in the range from 500°C to 900°C affected both the amplitude and the maximum value of the normalized deflection. The presented results demonstrate that through heat-treatment the functional properties of the analyzed Ni-Mn-Ga-Cu ribbons, obtained by the melt spinning method, can be effectively optimized.

Keywords: Shape memory alloys; microstructure; melt spinning; martensite

1. Introduction

In recent years, metallic materials based on ternary Ni-Mn-Ga alloys have been intensively studied, due to their unique combination of magnetic and mechanical properties [1,2]. These materials, in the single-crystalline state, can significantly change their shape at the macroscopic level under the influence of external magnetic field of about 1T [3-5]. This phenomenon is known as the magnetic field-induced straining (MFIS) effect, which occurs at the microscopic level through the reorientation of martensite variants via deformation twinning and detwinning mechanism [6-12]. In recent years, a great deal of research has been carried out to understand the fundamental properties of this phenomenon, which has consequently led to the modification of various material's characteristics that directly influence and may optimize the MFIS effect itself. The largest experimentally recorded MFIS effect of 12% of linear strain was observed in the Ni-Mn-Ga-Co-Cu alloy with the non-modulated martensite structure [13]. In the ternary Ni-Mn-Ga alloys, the effect of functional strain occurred only in the modulated martensite phases. Depending on the type of modulation [14-17], the maximum recorded linear strain was about 7% and 11%

in 10-fold (10M) and 14-fold modulated (14M) martensite structures, respectively [18,19].

Although, the highest recorded strain values, generated by the MFIS effect, were recorded in single-crystalline materials. There is currently a great deal of interest in the shape memory community to produce these materials in the poly-crystalline form using various production techniques. Such materials have been produced in the form of foams, microshells, microwires, etc. [20-27]. Consequently, this type of approach has led to a variety of interesting functional properties, e.g. microwires with the so-called oligo-crystalline microstructure, fabricated using the Taylor technique, have shown magnetic shape memory properties in the form of bending under the influence of an external magnetic field [28]. Magnetically field-induced bending (MFIB) has also been detected in single-crystalline Ni-Mn-Ga ternary alloys, which proven to be particularly important for materials with a large length-to-width ratio. A detailed experimental study by Kucza et al. [29] illustrates quantitatively the contributions of two components to the total functional strain: axial strain and bending strain, which were attributed to MFIS and MTIB (magnetic torque-induced bending) phenomena, respectively.

¹ INSTITUTE OF METALLURGY AND MATERIALS SCIENCE, POLISH ACADEMY OF SCIENCE, 25 REYMONTA STR., 30-059, KRAKÓW, POLAND

* Corresponding author: m.szczerba@imim.pl



An interesting and relatively readily available method for producing polycrystalline metallic materials from the liquid phase is the melt spinning technique, which produces material with high chemical homogeneity in the form of thin ribbons, tens of micrometers thick [30-32].

The MFIB effect was observed in Ni-Mn-Ga-Co-Cu alloys [33]. This material in the shape of a ribbon was obtained by rapid crystallization from the liquid phase using melt spinning technique. A characteristic material's feature obtained by this method is a strong anisotropy of the microstructure, where fine grains are located near the surface being in contact with the rotating wheel. In contrast, further away from the contact surface, the grains have more columnar shape [34,35]. The as-cast ribbons are also characterized by a significant level of residual stresses, which is often the reason for the reduced ductility of this material. In the case of Ni-Mn-Ga-based alloys, our previous studies have shown a strong tendency towards recrystallization, which occurs in the temperature range of 550°C-900°C [33]. This phenomenon is preceded by annealing observed at lower temperatures below 550°C. Also, the effect of annealing on the martensitic transformation temperature observed in these ribbons was thoroughly analyzed [36,37]. Taking this into account, the present work will focus on the analysis of the effect of annealing in the temperature range from 100° to 900°C on the MFIB properties of an alloy with the nominal composition of Ni₅₀Mn₃₀Ga₁₈Cu₂ produced by melt spinning. The 2 atomic % addition of Cu was intended to increase the temperature of martensitic transformation, and consequently, to increase the temperature range of its potential application.

2. Experimental procedure

The first stage of the experimental research was the preparation of a polycrystalline ingot with the nominal composition of Ni₅₀Mn₃₀Ga₁₈Cu₂ using high purity metals (Ni – 99.9+%, Mn – 99.9%, Ga – 99.99% and Cu – 99.99%). This process involved induction melting in an argon atmosphere followed by homogenization at 900°C for 72 hours under vacuum conditions. Then, this ingot has used to produce ribbons by the melt spinning technique. The linear velocity of the rotating copper wheel during the casting process was set at 20 m/s. Ribbons were then encapsulated in vacuum conditions using quartz tubes and annealed in the temperature range 100°C-900°C for a period of 30 minutes. The ribbons' chemical composition was Ni_{50.2}Mn_{29.6}Ga_{18.1}Cu_{2.1} being determined by energy dispersive spectroscopy using scanning electron microscope.

The characteristic martensitic transformation temperatures of the as-cast ribbons and those after heat-treatment were determined by differential scanning calorimetry measurements, using TAI DSC Q 1000 calorimeter, in the temperature range from –100°C to 100°C, at heating and cooling rates of 10 K/min. The martensitic start (Ms) and finish (Mf) temperatures were 79°C and 71°C, respectively, i.e. well above room temperature. Microstructure changes, such as mean grain size, were analyzed for

both cast and annealed ribbons using Thermo Scientific Scios 2 DualBeam scanning electron microscope observations by means of backscattered electron (BSE) mode under high vacuum conditions. For the microstructure observations, the ribbons were carefully grinded and then electro-polished using Struers A2 reagent.

Another set of as-cast as well as annealed ribbons in the temperature range 100°-900°C were prepared for experimental studies of the MFIB effect. Measurements were made using a self-made device, which allowed in-situ imaging of the degree of bending of the ribbons under the magnetic field ranging from 0 to 0.3T. To carry out these measurements, the ribbons were clamped between two aluminum blocks and then placed in the device's holder. During the measurements, at different stages of bending (i.e. different values of magnetic field), images of the samples were taken. The MFIB measurements performed at room temperature were carried out for up to 10 bending cycles.

3. Results and discussion

The as-cast ribbons had an average grain size of 5.8 μm (Figs. 1 and 2). The 30 minute annealing procedure at the temperature of up to 500°C did not significantly affect the grain size. Their average size was 6.1 μm, 6.3 μm and 6.7 μm for samples annealed at 100°C, 300°C and 500°C, respectively. Larger grain growth was recorded for 700°C and 900°C, where the grain growth process occurred increasing the grain size to 9.1 μm and 15.2 μm, respectively. These results indicate that recrystallization does not occur up to 500°C. On the other hand, in the lower temperature range of up to 500°C, microstructural annealing processes (e.g. vacancy and dislocation annihilation) should be expected [34].

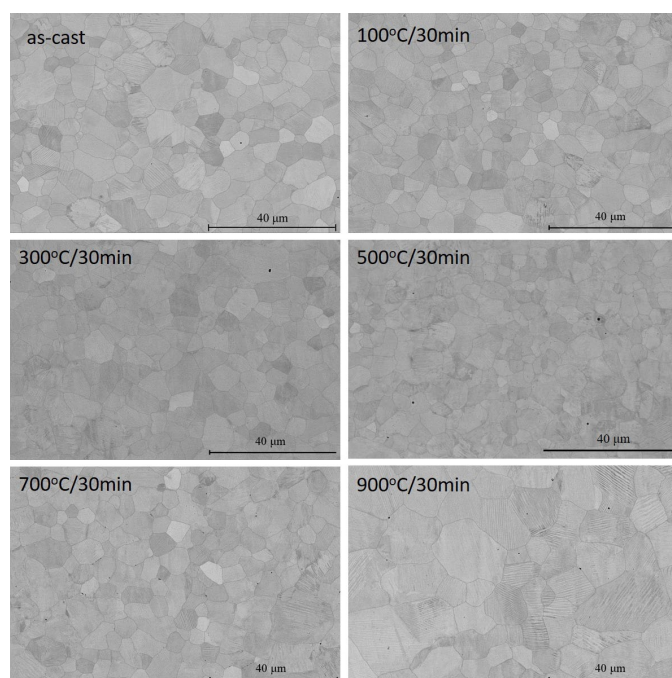


Fig. 1. Microstructure images taken in the BSE mode for the as-cast samples and annealed in the temperature range 100°C-900°C for 30 minutes

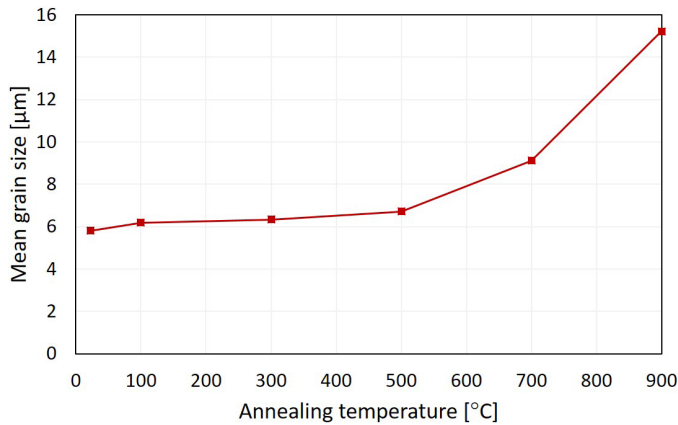


Fig. 2. Average grain size versus annealing temperature curve (in the range from 100°C to 900°C) for the ribbons with the nominal composition of $\text{Ni}_{50}\text{Mn}_{30}\text{Ga}_{18}\text{Cu}_2$

The initial MFIB experiments were performed for ribbons in the as-cast state (Fig. 3). In the first cycle, upon the initial increase of the magnetic field from 0 T to 0.14 T, a slight deflection of the ribbon occurred to a level of about 0.01. Further increase of the magnetic field up to 0.28 T generated a more significant bending effect of the normalized deflection (ND) parameter that reached 0.12. Decreasing the magnetic field resulted in a gradual decrease in the recorded ND to the level of 0.02 at zero magnetic field. Thus, the material did not return to its original shape after the first cycle, suggesting activation of plastic deformation mechanisms during MFIB. In the second cycle an increase of the magnetic field, in the same range as previously in the first cycle, also induced a gradual change in the ribbon's shape. The forth and back curve of the second cycle was characterized by a significantly smaller hysteresis and practically neglectable contribution of plastic deformation (the ribbon returned to its initial position).

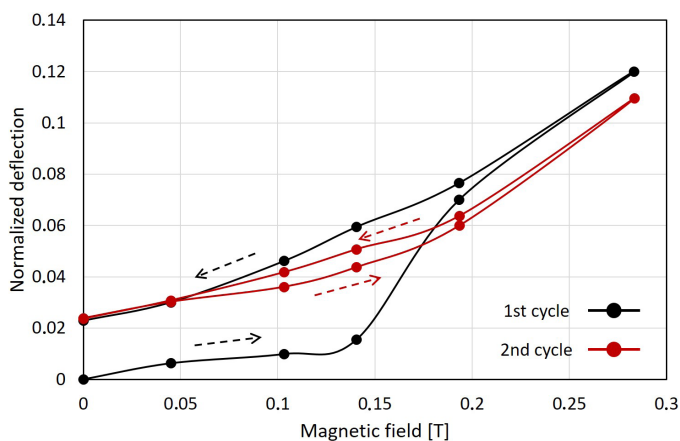


Fig. 3. Normalized deflection versus magnetic field curves obtained during the first and the second cycle of MFIB of the as-cast ribbons

The next stage of the study was to analyze the effect of annealing in the range from room temperature to 900°C on the effect of MFIB. Fig. 4 shows the MFIB data for the annealed ribbons at different temperatures of the initial cycle. In the range

up to 300°C, virtually no changes of the ribbon's behavior were observed. The maximum ND obtained for the as-cast ribbons and those annealed at 100°C and 300°C was approximately 0.12. A significant change in the curve occurred at 500°C, with an almost fourfold increase of the maximum ND reaching a value of 0.43. Annealing at 700°C and 900°C resulted in a further increase of ND to 0.65 and 0.75, respectively. Thus, the performed annealing process has a large effect on the MFIB of the analyzed ribbons, where the maximum value of ND increased by more than six-fold from 0.12 to 0.75. A significant effect of the annealing on the plastic contribution obtained in the first cycle can also be observed. For the as-cast ribbon, the ND was 0.03, while for the ribbon annealed at 900°C, this value reached 0.27. The second cycle was characterized by the absence of the plastic contribution during MFIB with the maximum ND remaining unchanged (Fig. 5). Also, for the second cycle, changes in the bending response can only be observed for ribbons annealed between 300°C and 900°C. By careful analysis of the first and the second cycle of the ribbons annealed at 900°C, it can be observed that the maximum value is around 0.75 (Fig. 6). The second cycle has a significantly smaller hysteresis loop and no plastic contribution (after the full second cycle the ND value was 0.27).

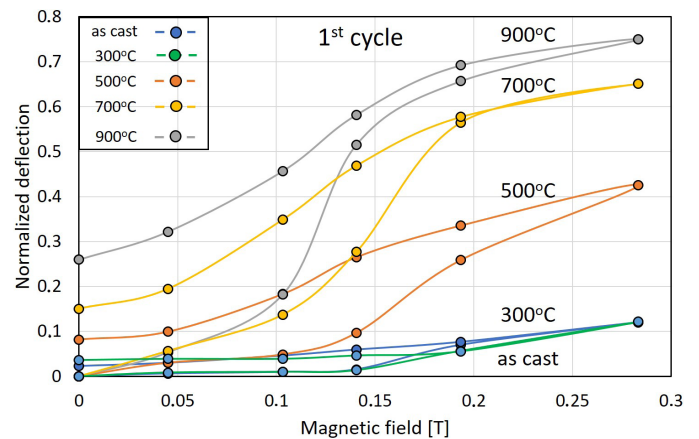


Fig. 4. Normalized deflection versus magnetic field curves during the first cycle of MFIB of the as-cast and annealed ribbons in the temperature range between 100°C and 900°C

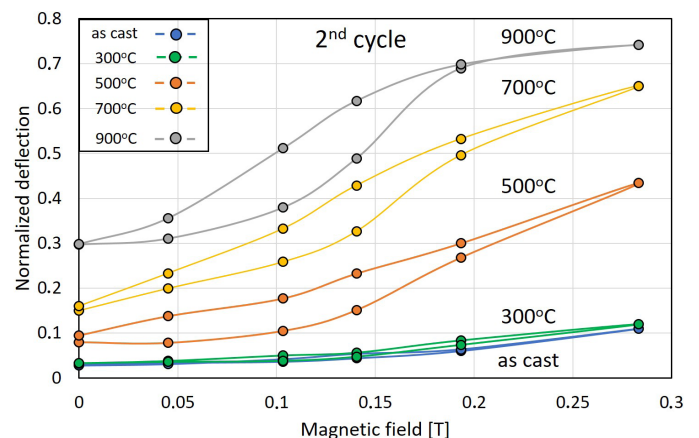


Fig. 5. Normalized deflection versus magnetic field curves of the second cycle of MFIB measurements of the as-cast and annealed ribbons in the temperature range between 100°C and 900°C

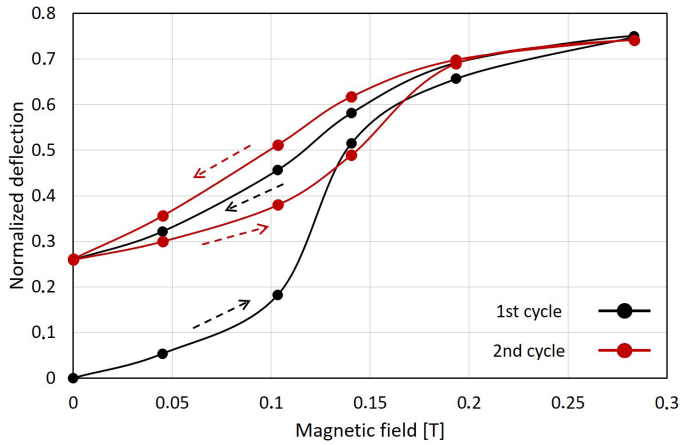


Fig. 6. Normalized deflection versus magnetic field curves during the first and the second cycle of MFIB of the annealed ribbons at 900°C for 30 minutes

The annealing process also influenced the value of the magnetic field that is necessary to activate the bending effect (Fig. 7). This value for the sample after casting in the first cycle was approximately 0.13T and decreased to 0.08T for the sample annealed at the highest temperature of 900°C. A similar trend is maintained for the second cycle with a general decrease in the magnetic field for the individual annealing temperature of about 0.02T.

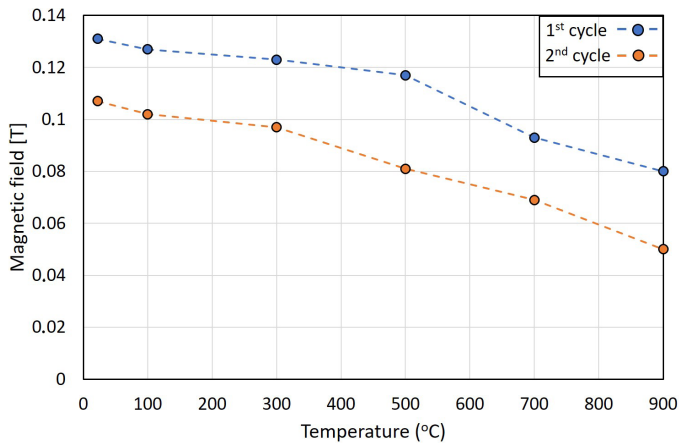


Fig. 7. The threshold value of the magnetic field versus annealing temperature curves for the first and second cycles required to initiate MFIB process of the analyzed ribbons

Fig. 8a shows the changes in maximum and minimum ND, which were recorded during 10 cycles. Significant differences can be seen in the ND values, depending on the annealing temperature (graphs for only three annealing conditions are shown in Fig. 8a for clarity). A good stability of the obtained effect with increasing cycle number is also evident. Based on the data shown in Fig. 8a, dependencies were evaluated for the changes in the maximum amplitude of the ND obtained as a function of annealing temperature (Fig. 8a). Again, up to 300°C, no changes in the amplitude were observed, which was about 0.07. Above this temperature, there was a significant increase in the

amplitude to a maximum value of 0.5. Thus, this increase must be attributed to the recrystallization process, and consequently, to the microstructural modification of the ribbons. A very similar effect of annealing can also be observed by analyzing the maximum ND values, which also remain unchanged up to 300°C (Fig. 8c). Above this temperature, there is an increase in ND reaching a maximum value of 0.74 for the ribbons annealed at 900°C.

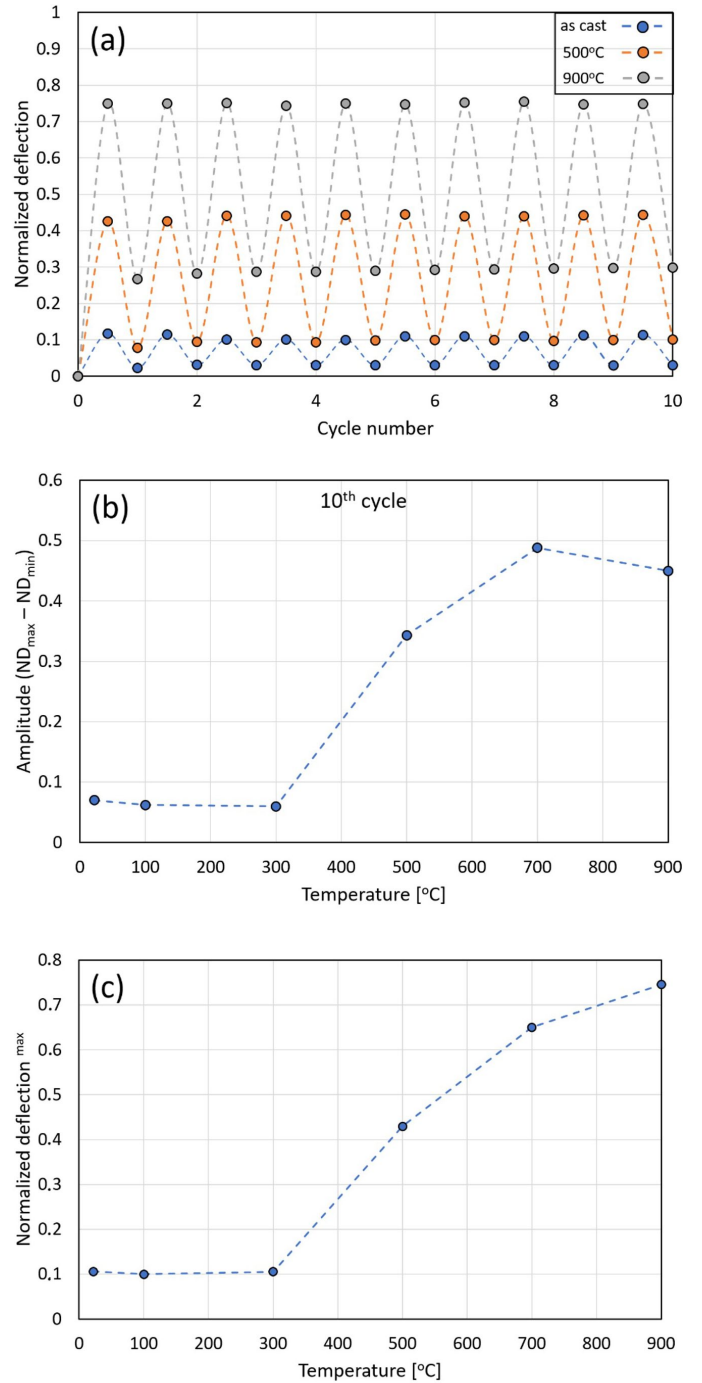


Fig. 8. Maximum and minimum normalized deflection versus cycle number curve of the as-cast and annealed ribbons at 500°C and 900°C (a), amplitude between the maximum and minimum value of the normalized deflection versus annealing temperature curve (b), and maximum value of the normalized deflection versus annealing temperature curve (c)

4. Conclusions

The presented experimental studies were focused on the effect of annealing on the functional properties of ribbons with the nominal composition of $\text{Ni}_{50}\text{Mn}_{30}\text{Ga}_{18}\text{Cu}_2$ produced by the melt spinning technique. The ribbons were annealed over a wide temperature range from 100°C to 900°C for 30 minutes. The annealing process resulted in an increase in average grain size from 5.8 μm for the as-cast sample to 15.2 μm for the one annealed at 900°C. The annealing process also affected the MFIB by a six-fold increase of the maximum ND value from the level of 0.12 to 0.75. However, this effect occurred for ribbons annealed at higher temperatures (500°C and above). The annealing process also reduced the value of the magnetic field required to activate the MFIB effect from the value of 0.13 T to 0.08 T for the first cycle. There was also further noticeable decrease in the magnetic field to 0.05 T for the second cycle. The effect of annealing between 500°C and 900°C affected the amplitude as well as the maximum value of ND. The results presented here show that by means of heat-treatment process (i.e. annealing for 30 minutes in the temperature range from 100°C to 900°C), the functional properties of the analyzed Ni-Mn-Ga-Cu ribbons obtained by melt spinning technique can be effectively optimized.

Acknowledgments

This work is funded by the Institute of Metallurgy and Materials Science of the Polish Academy of Science under the statutory work Z8.

REFERENCES

- [1] K. Ullakko, J.K. Huang, C. Kantner, R.C. O'Handley, V.V. Kokorin, Large magnetic-field-induced strains in Ni_2MnGa single crystals. *Appl. Phys. Lett.* **69**, 1966-1969 (1996). DOI: <https://doi.org/10.1063/1.117637>
- [2] P. Müllner, V.A. Chernenko, G. Kostorz, Stress-induced twin rearrangement resulting in change of magnetization in a Ni-Mn-Ga ferromagnetic martensite. *Scr. Mater.* **49** (2), 129-133 (2003). DOI: [https://doi.org/10.1016/S1359-6462\(03\)00219-7](https://doi.org/10.1016/S1359-6462(03)00219-7)
- [3] A.A. Likhachev, K. Ullakko, Magnetic-field-controlled twin boundaries motion and giant magneto-mechanical effects in Ni-Mn-Ga shape memory alloy. *Phys. Lett. Sect. A Gen. At. Solid State Phys.* **275** (1-2), 142-151 (2000). DOI: [https://doi.org/10.1016/S0375-9601\(00\)00561-2](https://doi.org/10.1016/S0375-9601(00)00561-2)
- [4] S.J. Murray, M. Marioni, S.M. Allen, R.C. O'Handley, T.A. Lograsso, 6% magnetic-field-induced strain by twin-boundary motion in ferromagnetic Ni-Mn-Ga. *Appl. Phys. Lett.* **77**, 886-888 (2000). DOI: <https://doi.org/10.1063/1.1306635>
- [5] P. Müllner, V.A. Chernenko, G. Kostorz, Large cyclic magnetic-field-induced deformation in orthorhombic (14M) Ni-Mn-Ga martensite. *J. Appl. Phys.* **95**, 1531-1536 (2004). DOI: <https://doi.org/10.1063/1.1639144>
- [6] B. Karki, P. Müllner, R. Pond, Topological model of type II deformation twinning in 10M Ni-Mn-Ga. *Acta Mater.* **201**, 604-616 (2020). DOI: <https://doi.org/10.1016/j.actamat.2020.10.020>
- [7] L. Straka, N. Lanska, K. Ullakko, A. Sozinov, Twin microstructure dependent mechanical response in Ni-Mn-Ga single crystals. *Appl. Phys. Lett.* **96**, 131903 (2010). DOI: <https://doi.org/10.1063/1.3373608>
- [8] R.C. Pond, B. Muntifering, P. Müllner, Deformation twinning in Ni_2MnGa . *Acta Mater.* **60** (9), 3976-3984 (2012). DOI: <https://doi.org/10.1016/j.actamat.2012.03.045>
- [9] R.C. Pond, J.P. Hirth, Topological model of type II deformation twinning. *Acta Mater.* **151**, 229-242 (2018). DOI: <https://doi.org/10.1016/j.actamat.2018.03.014>
- [10] S. Kustov, A. Saren, A. Sozinov, V. Kaminskii, K. Ullakko, Ultrahigh damping and Young's modulus softening due to a/b twins in 10M Ni-Mn-Ga martensite. *Scr. Mater.* **178**, 483-488 (2020). DOI: <https://doi.org/10.1016/j.scriptamat.2019.12.024>
- [11] L. Straka, O. Heczko, H. Seiner, N. Lanska, J. Drahokoupil, A. Soroka, S. Fähler, H. Hanninen, A. Sozinov, Highly mobile twinned interface in 10 M modulated Ni-Mn-Ga martensite: Analysis beyond the tetragonal approximation of lattice. *Acta Mater.* **59**, 7450-7463 (2011). DOI: <https://doi.org/10.1016/j.actamat.2011.09.020>
- [12] M.J. Szczerba, M.S. Szczerba, Transformation of dislocations during twin variant reorientation in Ni-Mn-Ga martensite structures. *Scr. Mater.* **66** (1), 29-32 (2012). DOI: <https://doi.org/10.1016/j.scriptamat.2011.09.034>
- [13] A. Sozinov, N. Lanska, A. Soroka, W. Zou, 12% magnetic field-induced strain in Ni-Mn-Ga-based non-modulated martensite. *Appl. Phys. Lett.* **102**, 021902 (2013). DOI: <https://doi.org/10.1063/1.4775677>
- [14] J. Pons, R. Santamarta, V.A. Chernenko, E. Cesari, Long-period martensitic structures of Ni-Mn-Ga alloys studied by high-resolution transmission electron microscopy. *J. Appl. Phys.* **97**, 083516 (2005). DOI: <https://doi.org/10.1063/1.1861137>
- [15] L. Righi, F. Albertini, L. Pareti, A. Paoluzi, G. Calestani, Commensurate and incommensurate "5M" modulated crystal structures in Ni-Mn-Ga martensitic phases. *Acta Mater.* **55** (15), 5237-5245 (2007). DOI: <https://doi.org/10.1016/j.actamat.2007.05.040>
- [16] J. Pons, R. Santamarta, V.A. Chernenko, E. Cesari, Structure of the layered martensitic phases of Ni-Mn-Ga alloys. *Mater. Sci. Eng. A* **438-440**, 931-934 (2006). DOI: <https://doi.org/10.1016/j.msea.2006.02.179>
- [17] J. Pons, V.A. Chernenko, R. Santamarta, E. Cesari, Crystal structure of martensitic phases in Ni-Mn-Ga shape memory alloys. *Acta Mater.* **48** (12), 3027-3038 (2000). DOI: [https://doi.org/10.1016/S1359-6454\(00\)00130-0](https://doi.org/10.1016/S1359-6454(00)00130-0)
- [18] E. Pagounis, R. Chulist, M.J. Szczerba, M. Laufenberg, Over 7% magnetic field-induced strain in a Ni-Mn-Ga five-layered martensite. *Appl. Phys. Lett.* **105**, 052405 (2014). DOI: <https://doi.org/10.1063/1.4892633>
- [19] E. Pagounis, M.J. Szczerba, R. Chulist, M. Laufenberg, Large magnetic field-induced work output in a NiMnGa seven-layered modulated martensite. *Appl. Phys. Lett.* **107**, 152407 (2015). DOI: <https://doi.org/10.1063/1.4933303>

- [20] A. Mostafaei, K.A. Kimes, E.L. Stevens, J. Toman, Y.L. Krimer, K. Ullakko, M. Chmielus, Microstructural evolution and magnetic properties of binder jet additive manufactured Ni-Mn-Ga magnetic shape memory alloy foam. *Acta Mater.* **131**(1), 482-490 (2017). DOI: <https://doi.org/10.1016/j.actamat.2017.04.010>
- [21] A. Mostafaei, P. Rodriguez De Vecchis, E.L. Stevens, M. Chmielus, Sintering regimes and resulting microstructure and properties of binder jet 3D printed Ni-Mn-Ga magnetic shape memory alloys. *Acta Mater.* **154**, 355-364 (2018). DOI: <https://doi.org/10.1016/j.actamat.2018.05.047>
- [22] M. Chmielus, X.X. Zhang, C. Witherspoon, D.C. Dunand, P. Müllner, Giant magnetic-field-induced strains in polycrystalline Ni-Mn-Ga foams. *Nat. Mater.* **8** (11), 863-866 (2009). DOI: <https://doi.org/10.1038/nmat2527>
- [23] D. Musiienko, A. Saren, L. Straka, M. Vronka, J. Kopeček, O. Heczko, A. Sozinov, Kari Ullakko, Ultrafast actuation of Ni-Mn-Ga micropillars by pulsed magnetic field. *Scr. Mater.* **162**, 482-485 (2019). DOI: <https://doi.org/10.1016/j.scriptamat.2018.12.009>
- [24] T.-F.M. Chang, V. Chernenko, H.-C. Tang, C.-Y. Chen, A. Umise, M. Tahara, H. Hosoda, M. Sone, Superelastic behavior of single crystalline Ni₄₈Fe₂₀Co₅Ga₂₇ micro-pillars near austenite–martensite critical point. *AIP Adv.* **11**, 025213 (2021). DOI: <https://doi.org/10.1063/5.0036304>
- [25] F. Lambrecht, N. Sagardiluz, M. Gueltig, I.R. Aseguinolaza, V.A. Chernenko, M. Kohl, Martensitic transformation in NiMnGa/Si bimorph nanoactuators with ultra-low hysteresis. *Appl. Phys. Lett.* **110**, 213104 (2017). DOI: <https://doi.org/10.1063/1.4984058>
- [26] Y. Zhao, M. Kang, J. Xue, J. Ju, M. Wang, S. Wang, Y. Zhang, M. Vazquez, H. Gao, J. Wang, Strain-magnetization effect in superelastic Ni-Mn-Ga microfiber. *Scr. Mater.* **162**, 397-401 (2019). DOI: <https://doi.org/10.1016/j.scriptamat.2018.12.002>
- [27] H. Hosoda, J. Lazarczyk, P. Sratong-on, M. Tahara, V. Chernenko, Elaboration of magnetostrain-active NiMnGa particles/polymer layered composites. *Mater. Lett.* **289**, 129427 (2021). DOI: <https://doi.org/10.1016/j.matlet.2021.129427>
- [28] P. Zheng, N.J. Kucza, C.L. Patrick, P. Müllner, D.C. Dunand, Mechanical and magnetic behavior of oligocrystalline Ni–Mn–Ga microwires. *J. Alloy. Compd.* **624**, 226-233 (2015). DOI: <https://doi.org/10.1016/j.jallcom.2014.11.067>
- [29] N.J. Kucza, C.L. Patrick, D.C. Dunand, P. Müllner, Magnetic-field-induced bending and straining of Ni–Mn–Ga single crystal beams with high aspect ratios. *Acta Mater.* **95**, 284-290 (2015). DOI: <https://doi.org/10.1016/j.actamat.2015.05.030>
- [30] E. Villa, O. Aguilar-Ortiz, A. Nespoli, P. Alvarez-Alonso, J.P. Camarillo-Garcia, D. Salazar, F. Passaretti, H. Flores-Zuniga, H. Hosoda, V.A. Chernenko, Tailoring thermomechanical treatment of Ni-Fe-Ga melt-spun ribbons for elastocaloric applications. *J. Mater. Res. Technol.* **8** (5), 4540-4546 (2019). DOI: <https://doi.org/10.1016/j.jmrt.2019.07.067>
- [31] Y. Wu, J. Wang, Y. He, H. Wu, C. Jiang, H. Xu, Microstructure and the correlated martensitic transformation of melt spinning Ni₅₀Mn₂₉Ga_{21-x}Tb_x (x = 0–1) ribbons. *Acta Mater.* **104**, 91-100 (2016). DOI: <https://doi.org/10.1016/j.actamat.2015.11.043>
- [32] V. Golub, I.R. Aseguinolaza, O. Salyuk, D. Popadiuk, I. Sharay, R. Fernandez, V. Alexandrakis, S.A. Bunyaev, G.N. Kakazei, J.M. Barandiaran, V.A. Chernenko, Thickness dependences of structural and magnetic properties of Ni (Co)MnSn/MgO(001) thin films. *J. Alloy. Compd.* **862**, 158474 (2021). DOI: <https://doi.org/10.1016/j.jallcom.2020.158474>
- [33] M.J. Szczerba, Giant magnetic-field-induced bending effect in Ni-Mn-Ga-Co-Cu melt-spun ribbons. *Scripta Mater.* **205**, 114203 (2021). DOI: <https://doi.org/10.1016/j.scriptamat.2021.114203>
- [34] A. Brzoza, M. Kowalczyk, A. Wierzbicka-Miernik, P. Czaja, W. Maziarz, A. Wójcik, J. Wojewoda-Budka, M. Sikora, J. Dutkiewicz, M.J. Szczerba, Microstructural anisotropy, phase composition and magnetic properties of as-cast and annealed Ni-Mn-Ga-Co-Cu melt-spun ribbons. *J. Alloy. Compd.* **776**, 319-325 (2019). DOI: <https://doi.org/10.1016/j.jallcom.2018.10.231>
- [35] P. Czaja, M. Kowalska, A. Brzoza-Kos, M.J. Szczerba, Mechanical response during bending of Ni–Mn–Ga-based melt-spun ribbons. *J. Mater. Sci.* **57**, 16923-16929 (2022). DOI: <https://doi.org/10.1007/s10853-022-07690-y>
- [36] M. Kowalska, P. Czaja, T. Czeppe, Ł. Rogal, M.J. Szczerba, Anisotropy and Temperature Dependence of Annealing During Mechanical Bending in Ni-Mn-Ga-Based Melt-Spun Ribbons. *J. of Materi. Eng. and Perform.* **34**, 3800-3810 (2025). DOI: <https://doi.org/10.1007/s11665-024-10524-4>
- [37] M. Kowalska, P. Czaja, Ł. Rogal, M.J. Szczerba, Effect of Linear Velocity on Magneto-mechanical Properties of Ni-Mn-Ga-Based Melt-Spun Ribbons. *Metall. Mater. Trans. A* **55**, 4653-4662 (2024). DOI: <https://doi.org/10.1007/s11661-024-07585-4>